Nominal High-Altitude Electromagnetic Pulse (HEMP) Waveforms

Technical Report

Submitted by:

Applied Research Associates, Inc.

January 2019

REPORT DOCUMENTATION PAGE

Form Approved
OMB No. 0704-0188

Public reporting burden for this collection of information is estimated to average 1 hour per response, including the time for reviewing instructions, searching existing data sources, gathering and maintaining the   data needed, and completing and reviewing this collection of information. Send comments regarding this burden estimate or any other aspect of this collection of information, including suggestions for reducing   this burden to Department of Defense, Washington Headquarters Services, Directorate for Information Operations and Reports (0704-0188), 1215 Jefferson Davis Highway, Suite 1204, Arlington, VA 22202-   4302. Respondents should be aware that notwithstanding any other provision of law, no person shall be subject to any penalty for failing to comply with a collection of information if it does not display a currently   valid OMB control number. **PLEASE DO NOT RETURN YOUR FORM TO THE ABOVE ADDRESS.**

1. REPORT DATE *(DD-MM-YYYY)*	2. REPORT TYPE	3. DATES COVERED *(From - To)*
14-01-2019	Technical Report	November 2018 – January 2019

4. TITLE AND SUBTITLE	5a. CONTRACT NUMBER
	HDTRA1-14-D-0003-0016
Nominal High-Altitude Electromagnetic Pulse (HEMP) Waveforms	5b. GRANT NUMBER
	5c. PROGRAM ELEMENT NUMBER

6. AUTHOR(S)	5d. PROJECT NUMBER
Jonathan Morrow-Jones	
	5e. TASK NUMBER
	5f. WORK UNIT NUMBER

7. PERFORMING ORGANIZATION NAME(S) AND ADDRESS(ES) AND ADDRESS(ES)	8. PERFORMING ORGANIZATION REPORT NUMBER
Applied Research Associates 5425 Hollister Avenue Suite 220 Santa Barbara, CA 93111	ARA-FPEMP-NOMINAL-HEMP

9. SPONSORING / MONITORING AGENCY NAME(S) AND ADDRESS(ES)	10. SPONSOR/MONITOR'S ACRONYM(S)
Defense Threat Reduction Agency/RD-NTE 8725 John J. Kingman Rd., Stop 6201 Ft. Belvoir, VA 22060-6201	DTRA/RD-NTE
	11. SPONSOR/MONITOR'S REPORT NUMBER(S) DTRA-TR-19-XXX

12. DISTRIBUTION / AVAILABILITY STATEMENT
DISTRIBUTION A. Approved for public release. Distribution unlimited.

13. SUPPLEMENTARY NOTES

14. ABSTRACT
The report explores the maximum early-time, high-altitude electromagnetic pulse, referred to as HEMP E1, using unclassified, published gamma-ray spectra, and a fixed time dependence for gamma-ray rate. The report shows how predicted HEMP E1 varies with yield, gamma spectrum, height of burst, and latitude. The report provides calculated maximum incident HEMP E1 as a function of yield.

15. SUBJECT TERMS
Electromagnetic Pulse · EMP · High-Altitude EMP · Waveforms · Gamma Ray · Spectrum · Early-Time HEMP · HEMP E1

16. SECURITY CLASSIFICATION OF:			17. LIMITATION OF ABSTRACT	18. NUMBER OF PAGES	19a. NAME OF RESPONSIBLE PERSON
a. REPORT Unclassified	**b. ABSTRACT** Unclassified	**c. THIS PAGE** Unclassified	Unclassified	21	Mark Sward **19b. TELEPHONE NUMBER** *(include area code)* 703-767-2525

Standard Form 298 (Rev. 8-98)
Prescribed by ANSI Std. Z39.18

UNIT CONVERSION TABLE
U.S. customary units to and from international units of measurement[*]

U.S. Customary Units	Multiply by →	← Divide by[†]	International Units
Length/Area/Volume			
inch (in)	2.54	$\times 10^{-2}$	meter (m)
foot (ft)	3.048	$\times 10^{-1}$	meter (m)
yard (yd)	9.144	$\times 10^{-1}$	meter (m)
mile (mi, international)	1.609 344	$\times 10^{3}$	meter (m)
mile (nmi, nautical, U.S.)	1.852	$\times 10^{3}$	meter (m)
barn (b)	1	$\times 10^{-28}$	square meter (m^2)
gallon (gal, U.S. liquid)	3.785 412	$\times 10^{-3}$	cubic meter (m^3)
cubic foot (ft^3)	2.831 685	$\times 10^{-2}$	cubic meter (m^3)
Mass/Density			
pound (lb)	4.535 924	$\times 10^{-1}$	kilogram (kg)
unified atomic mass unit (amu)	1.660 539	$\times 10^{-27}$	kilogram (kg)
pound-mass per cubic foot (lb ft^{-3})	1.601 846	$\times 10^{1}$	kilogram per cubic meter (kg m^{-3})
pound-force (lbf avoirdupois)	4.448 222		newton (N)
Energy/Work/Power			
electron volt (eV)	1.602 177	$\times 10^{-19}$	joule (J)
erg	1	$\times 10^{-7}$	joule (J)
kiloton (kt) (TNT equivalent)	4.184	$\times 10^{12}$	joule (J)
British thermal unit (Btu) (thermochemical)	1.054 350	$\times 10^{3}$	joule (J)
foot-pound-force (ft lbf)	1.355 818		joule (J)
calorie (cal) (thermochemical)	4.184		joule (J)
Pressure			
atmosphere (atm)	1.013 250	$\times 10^{5}$	pascal (Pa)
pound force per square inch (psi)	6.984 757	$\times 10^{3}$	pascal (Pa)
Temperature			
degree Fahrenheit (°F)	[T(°F) − 32]/1.8		degree Celsius (°C)
degree Fahrenheit (°F)	[T(°F) + 459.67]/1.8		kelvin (K)
Radiation			
curie (Ci) [activity of radionuclides]	3.7	$\times 10^{10}$	per second (s^{-1}) [becquerel (Bq)]
roentgen (R) [air exposure]	2.579 760	$\times 10^{-4}$	coulomb per kilogram (C kg^{-1})
rad [absorbed dose]	1	$\times 10^{-2}$	joule per kilogram (J kg^{-1}) [gray (Gy)]
rem [equivalent and effective dose]	1	$\times 10^{-2}$	joule per kilogram (J kg^{-1}) [sievert (Sv)]

[*]Specific details regarding the implementation of SI units may be viewed at http://www.bipm.org/en/si/.

[†]Multiply the U.S. customary unit by the factor to get the international unit. Divide the international unit by the factor to get the U.S. customary unit.

Table of Contents

List of Tables

List of Figures

1 INTRODUCTION

Even before the Trinity nuclear test in July of 1945, physicists predicted a transient electromagnetic signal would be caused by high-energy photons released from the detonation interacting with the air around the detonation. Predictions of these signals were difficult to make due to the complexity of the physics unleashed by the detonation [1].

Post World War II, there was a period of active atmospheric nuclear testing until 1962 [2], during which measurements of these signals were made in order to understand the phenomena that were previously largely viewed as an annoyance and impediment to other instrumentation. The name "electromagnetic pulse" (EMP) began to be used to refer to these signals.

EMP is a complex nonlinear phenomenon. Initially, it was observed that signal strengths grew weaker with increasing burst heights, but this trend did not continue as burst heights went ever higher: rather, a new, and faster signal was observed. This new signal was estimated ahead of the high-altitude tests of 1962 by William Karzas and Richard Latter [3]; without an adequate theory for this high-altitude EMP (HEMP) phenomenon, however, experimenters and the instrumentation teams had a difficult time collecting the signal on scale. With the end of atmospheric testing, so ended the acquisition of HEMP experimental data.

HEMP waveform can be notionally decomposed into three major timescales: early time (E1), intermediate time (E2), and late time (E3). These are depicted in Figure 1. The early time component, E1, is caused by the prompt, unscattered gamma rays emitted from the nuclear explosion. The intermediate time component, E2, is decomposed into two different parts for high-altitude detonations: the first part of E2, referred to as E2A, is a continuation of E1. The second part of E2, called E2B, is caused by high-energy neutrons interacting with the atmosphere. Historically, these have been separated due to the different physics models used to predict HEMP in these different time regimes. The late-time component, E3, is also divided into two subcomponents. The first only appears from detonation altitudes above about 250 km. It is called E3 "blast" and is often labeled E3A. It is caused by the expanding debris from the detonation pushing against the earth's geomagnetic field. The second subcomponent of E3 is called E3 "heave" and is often labeled E3B. It is caused by x-ray and kinetic energy from the detonation heating and ionizing the upper atmosphere. The heating causes the atmosphere to expand and begin rising buoyantly. The ionization, combined with the buoyant rise, attempts to pull the ions across geomagnetic field lines, creating a "heave."

The physics of E1 and E2 are dominated by nuclear physics of the interaction of the radiation output of the exploding nuclear weapon with the atmosphere. E3 is dominated by the magnetohydrodynamics (MHD) of energetic plasmas interacting with the earth's geomagnetic field.

This report focuses on E1. The objective is to demonstrate the dependence of HEMP E1 waveforms on yield, burst altitude, and latitude using open sources to derive the E1 waveforms.
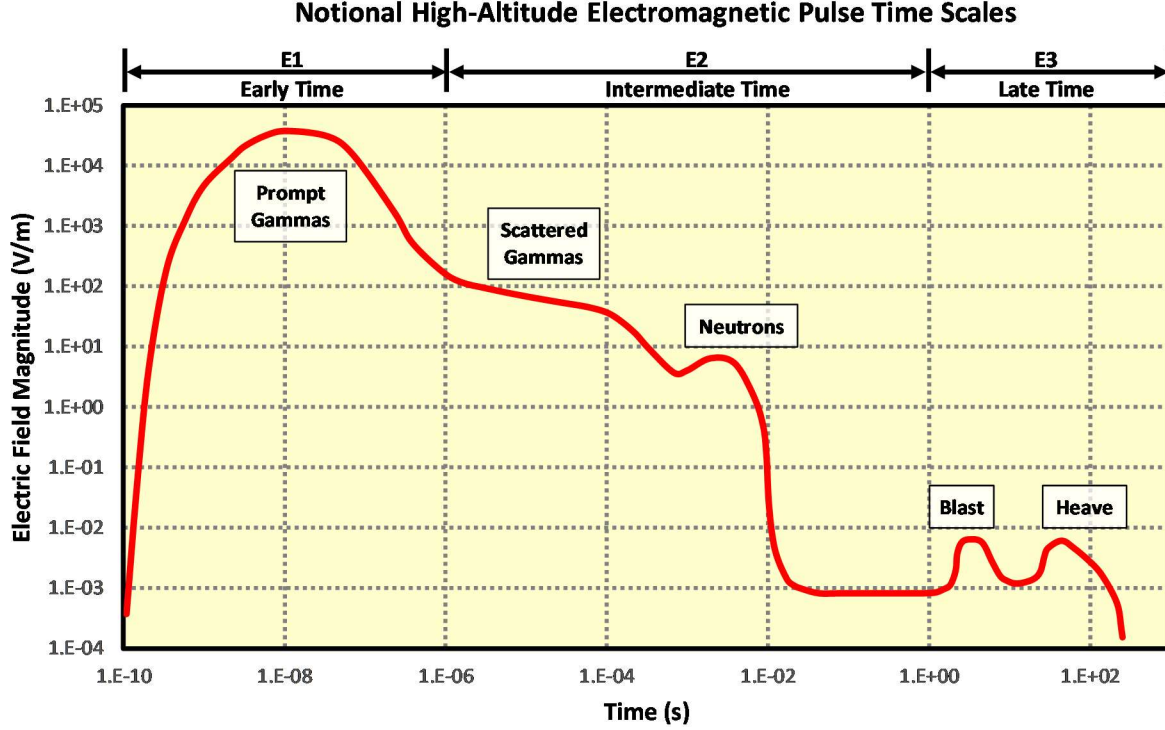
Notional High-Altitude Electromagnetic Pulse Time Scales

Figure 1. Example timescales for high-altitude electromagnetic pulse (HEMP).

2   THEORY OF EARLY-TIME HEMP WAVEFORMS

The theory of high-altitude, fast electromagnetic pulse signal starts from the idea that an electromagnetic current from a nuclear detonation is produced due to the mostly-radial outward movement of recoil electrons from *Compton scattering*. In Compton scattering, a gamma-ray from the nuclear detonation "collides" with an electron. This interaction causes the gamma-ray to transfer energy to the electron, and moves the electron in a different direction. The outward-moving Compton recoil electrons are also turned as they cross the geomagnetic field lines. The net motion of the electrons is the outward motion (radial) from the detonation plus transverse components from turning in the geomagnetic field. As they traverse through air, these electrons continue to interact with the air, depositing energy into the air or ionizing air molecules, creating conductivity. The amplitude and waveform shape of the electromagnetic pulse are therefore the result of the competition between the creation of the electrical current, which generates the electromagnetic fields, and the creation of conductivity, which dampens electromagnetic fields.

2.1   Electromagnetic Equations

The starting point for understanding HEMP is the two Maxwell's equations for the dynamics of the electric and magnetic fields [4]: in MKS units, they are

$$\frac{\partial \mathbf{B}}{\partial t} = -\nabla \times \mathbf{E}\,, \tag{1}$$

$$\epsilon_0 \frac{\partial \mathbf{E}}{\partial t} = \frac{1}{\mu_0}\nabla \times \mathbf{B} - \mathbf{J}_C - \sigma\mathbf{E}\,. \tag{2}$$

2

Here $\mathbf{E}$ is the electric field in volts per meter (V/m), $\mathbf{B}$ the magnetic field in tesla (T), $\mathbf{J}_c$ is the Compton current density in ampere per square meter (A/m^2), ϵ_0 is the permittivity (also called the dielectric constant) of free space, μ_0 is the permeability of free space[1], and σ is the time-dependent conductivity of the medium (for HEMP, it is that of air in the atmosphere, temporarily altered by the nuclear explosion, referred to as the "source region").

There are two additional equations in the set of Maxwell's equations:

$$\epsilon_0 \nabla \cdot \mathbf{E} = \rho \,, \tag{3}$$

$$\nabla \cdot \mathbf{B} = 0 \,. \tag{4}$$

Here ρ is the charge density in coulomb per cubic meter. These equations provide the constraints that Equations (1) and (2) must satisfy.

Equation (2) is where the fields are generated through the Compton current, $\mathbf{J}_C$, and damped through the conductivity, σ. The Compton current $\mathbf{J}_C$ satisfies the continuity equation

$$\nabla \cdot \mathbf{J} + \frac{\partial \rho}{\partial t} = 0, \tag{5}$$

where

$$\mathbf{J} = \mathbf{J}_C + \sigma \mathbf{E} \,. \tag{6}$$

The EMP fields $\mathbf{E}$ and $\mathbf{B}$ in time, sometimes referred to as the "waveform", are obtained as the solution of Maxwell's equations. To solve Maxwell's equations, however, one will need the current $\mathbf{J}_C$ and the conductivity σ.

2.2   Current Source Term

The source current term, $\mathbf{J}_C$, arises from the recoil of electrons produced from the interactions of the high-energy photons (gamma rays or x-rays) released from the nuclear explosion with the surrounding air molecules. The dominant interaction is Compton scattering. The scattered photons can interact with electrons in air again in secondary or higher-order scattering. Other effects can also produce electrons that contribute to $\mathbf{J}_C$. Due to the dominance of Compton scattering, the source term is sometimes referred to as the Compton current.

In tracking the motions of electrons, there are two main forces to consider: electromagnetic fields acting through the classical Lorentz force, or the electromagnetic force acted upon the electrons, and the transfer of energy to atomic electrons. The latter force arises through the scattering of recoil electrons in surrounding air and the associated (linear) energy transfer. This is often treated in an averaged form (for example, as a beam). As the individual electrons undergo scattering, they lose their initial common direction (deviating from a "beam") and begin to have increasing divergent, random transverse velocities. This increasing random transverse motions of the electrons is tracked through a term called obliquity, η, which is a function of the angle of deviation of the individual electrons from the mean direction (that is, how far the individual electrons have bent from the "core" of the beam). HEMP E1 simulation codes track the evolution of the obliquity through a separate dynamic equation or they do a Monte Carlo tracking of the individual electrons.

---

[1] Note that the permittivity and the permeability of the free space can be related to speed of light in vacuum, c (in meters per second): $c^2 \mu_0 \epsilon_0 = 1$.

The electromagnetic fields for the Lorentz force include both the geomagnetic fields as well as the fields generated by the motion of the recoil electrons. This is one of the ways in which HEMP E1 is a nonlinear phenomenon.

A treatment of the Compton current can be found in [5].

2.3 Time-Dependent Air Conductivity

As the Compton recoil electrons move through air and undergo multiple scatterings, they ionize the surrounding air, knocking electrons off air molecules and producing ions, and in the process making conduction electrons. This conductivity, σ, is time-varying function of the electron-ion pairs production rate (ionization rate) and the property of the air, including its density, temperature, and water content, how fast electrons attach to components of air molecules, and the mobility of the electrons and ions in the air. For E1 HEMP, the conductivity is

$$\sigma = e\big(\mu_e\, n_e + \mu_i\, (n_- + n_+)\big), \tag{7}$$

where μ_e is the electron mobility, μ_i is the ion mobility, n_e is the electron density, and n_- and n_+ are the negative and positive ion densities, respectively. The electron mobility depends on conduction electron collision frequencies, and in turn they depend on the electric field. Thus, the conductivity introduces yet another nonlinearity to the HEMP problem. Very late-time conductivity will depend on ionic conductivity once conduction electrons have mostly attached to neutral atoms or molecules, or have recombined with positive ions. However, for HEMP E1, the ionic conductivity can generally be ignored.

Air conductivity or air chemistry is an area of active research. An early study can be found in [6]. A time-dependent ionization modeled was studied in detail in [7]; at the completion of ionization, an energetic Compton recoil electron may produce about 30,000 conduction electrons in a finite period of time. The process of attachment of ionization electrons to oxygen and nitrogen in air was studied in [8]; the key modeling parameters being the reaction rates for the production and depletion of ions. Finally, the mobility of the electrons and ions were treated as empirically-derived constants, see [9].

2.4 High-Frequency Approximation

Equations (1) and (2) would be very difficult to solve over the scale of HEMP, which can be continental scales and several tens of kilometers of atmosphere. The method outlined in Longley and Longmire [10] first puts Equations (1) and (2) in spherical coordinates (r, θ, ϕ) centered at the burst point and in *retarded time* τ, defined by $\tau = t - r/c$. The electric and magnetic fields are also rewritten in terms of their radial components, E_r and B_r, and outgoing and ingoing fields, F and G, respectively:

$$F_1 \equiv r\big(E_\theta + cB_\phi\big), \tag{8}$$

$$F_2 \equiv r\big(E_\phi - cB_\theta\big), \tag{9}$$

$$G_1 \equiv r\big(E_\theta - cB_\phi\big), \tag{10}$$

$$G_2 \equiv r\big(E_\phi + cB_\theta\big). \tag{11}$$

Longley and Longmire then simplified the problem by treating the solution as rays emanating from the burst point. This high-frequency approximation (HFA) assumes the main fields are dominated by outward-directed waves. The resulting Maxwell's equations are

$$\frac{\partial B_r}{\partial \tau} = 0 \, , \tag{12}$$

$$\frac{\partial E_r}{\partial \tau} + \frac{\sigma E_r}{\epsilon_0} = -\frac{J_r}{\epsilon_0} \, , \tag{13}$$

$$\frac{\partial G_1}{\partial \tau} + \frac{\sigma G_1}{4\epsilon_0} = -\frac{r J_\theta}{2\epsilon_0} - \frac{\sigma F_1}{4\epsilon_0} \, , \tag{14}$$

$$\frac{\partial G_2}{\partial \tau} + \frac{\sigma G_2}{4\epsilon_0} = -\frac{r J_\phi}{2\epsilon_0} - \frac{\sigma F_2}{4\epsilon_0} \, , \tag{15}$$

$$\frac{\partial F_1}{\partial r} + \frac{\sigma F_1}{2c\epsilon_0} = -\frac{r J_\theta}{c\epsilon_0} - \frac{\sigma G_1}{2c\epsilon_0} \, , \tag{16}$$

$$\frac{\partial F_2}{\partial r} + \frac{\sigma F_2}{2c\epsilon_0} = -\frac{r J_\phi}{2c} - \frac{\sigma G_2}{2c\epsilon_0} \, . \tag{17}$$

The HFA formulation has proven very effective for capturing the early part of the HEMP waveform and is amenable to numerical solutions on computers. The CHAP code [10], first developed in the 1970's, continues to be the intellectual backbone of most, if not all, software tools for HEMP modeling ever since.

2.5 Qualitative Description of HEMP E1 Fields Using HFA

The predominant features of HFA approximation of Maxwell's equations are the outgoing transverse fields, F_1 and F_2, whose evolution are represented by Equations (16) and (17). These two equations describe the electromagnetic fields that are building up as they propagate outward along rays emanating from the detonation.

A feature of Equations (14) -- (17) is that the ingoing and outgoing fields satisfy differential equations whose source terms are components of the net current $\mathbf{J} = \mathbf{J}_c + \sigma\mathbf{E}$. Since recoil electrons happen ahead of ionization, the rise of the recoil current term tends to be a little ahead of the rise of the conducting electrons. The largest magnitude of the electric field, therefore, depends on the delicate timing between these two competing terms. In general, when $\mathbf{E} > \mathbf{J}_c/\sigma$, the EMP fields no longer grow, and instead are attenuated. This is sometimes referred to as a *saturated* field.

While HFA makes the HEMP problem computationally accessible, it brings with it certain assumptions and limitations. The HFA assumes angular dependence of gamma ray outputs from a nuclear weapon detonation are weak enough to be negligible. The electric field in the HFA approximation should scale like the inverse distance squared $(1/r^2)$ closer in to the source. Far away from the burst, solutions to Equations (12) -- (17) outside the source region always fall off like inverse distance $(1/r)$ thus only represent the radiated terms. The transition from close-in fields to radiated field depends on wavelength, or equivalently timescale. In general, the high-frequency approximation may break down for time scales greater than about 20 μs to 25 μs, or for altitudes below 20 km.

3   NOMINAL NUCLEAR WEAPON GAMMA OUTPUT

In order to calculate the source current term for the HEMP numerical modeling for a specific weapon, we need the output of that nuclear weapon. The components of the output most relevant to the HEMP calculations are the gamma spectrum (gamma-ray count per energy, for a range of energies) and the "gamma-dot" (the rate of gamma-rays escaping the exploding weapon, as a function of time). For most of the modeling and simulation of HEMP, these outputs come from nuclear weapons physics performance calculations carried out by those with knowledge of the design of nuclear weapons explosive packages, namely, by Department of Energy's Los Alamos and Lawrence Livermore National Laboratories[2].

In general, in a nuclear explosion, the energy released as prompt radiation is about 70% is x-rays, 1% neutrons, and 0.3% gamma rays [11]. The gamma rays are largely responsible for the generation of HEMP. For the purposes of this study, the fraction is set to 0.2%.

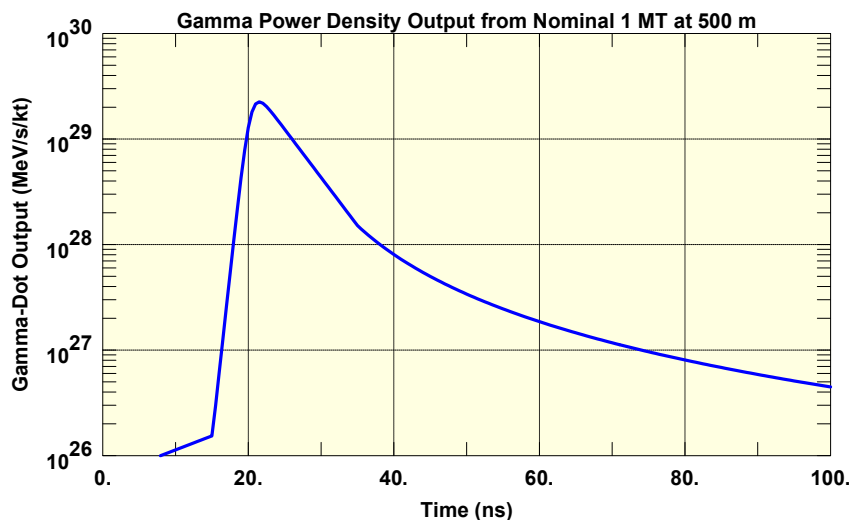## 3.1   Selecting a Gamma Time History

Figure 2. Gamma output rate as a function of time at 500 m from a nominal 1 MT high-altitude detonation (from [11], Figure 8.14).

The gamma rate time history is intimately tied to the performance characteristics of the nuclear weapon. The only known unclassified, published nuclear weapons gamma output time history is from Glasstone [11]. The plot in Glasstone, Figure 8.14, provides two time-dependent characteristics for the rate of gamma output, called gamma-dot ($\dot{\gamma}$). One curve is for a nominal 1 MT detonation near the surface at a distance of 500 m. That curve involves complex interactions with the ground. The second curve gives the gamma-dot time history for a high-altitude detonation. Although the second curve also represents some scattering, the early part of the time history should reasonably represent the prompt gamma-ray output from the detonation. This is shown in Figure 2. While the physics behind generating gamma-ray output suggests there may be a different time

---

[2] Historically, the weapons physics laboratories have provided model (that is, calculated) output information to DTRA and its predecessors for the modeling of effects of nuclear weapons such as blast, shock, and EMP. The weapons output would be tallied at a prescribed distance from the nuclear weapons explosion for a suitable period of time; this output would be handed to DTRA as the "input" or "source" for effects calculations and modeling.

dependence from one part of the gamma-ray spectrum to another, the time history depicted in Figure 2 will be used independent of gamma energy.

The gamma-dot time history is absolutely essential for HEMP calculations. In the absence of gamma-dot time histories that have a corresponding gamma spectrum, a scaling by yield is used to provide the necessary input to the HEMP calculation, but that also presents significant assumptions about the weapons characteristics, thus the results should be used with extreme caution.

3.2   Selecting a Gamma Spectrum

A number of unclassified nuclear weapons gamma spectra (that is, gamma output as a function of energy) are available, including Glasstone [11] and those of the Fat Man and Little Boy devices modeled by White et al [12]. Kramer et al [13] compare a number of gamma spectra from different sources, including those published by White et al, see [12]. Note that their gross shapes are all similar despite the fact that they derive from very different sources.
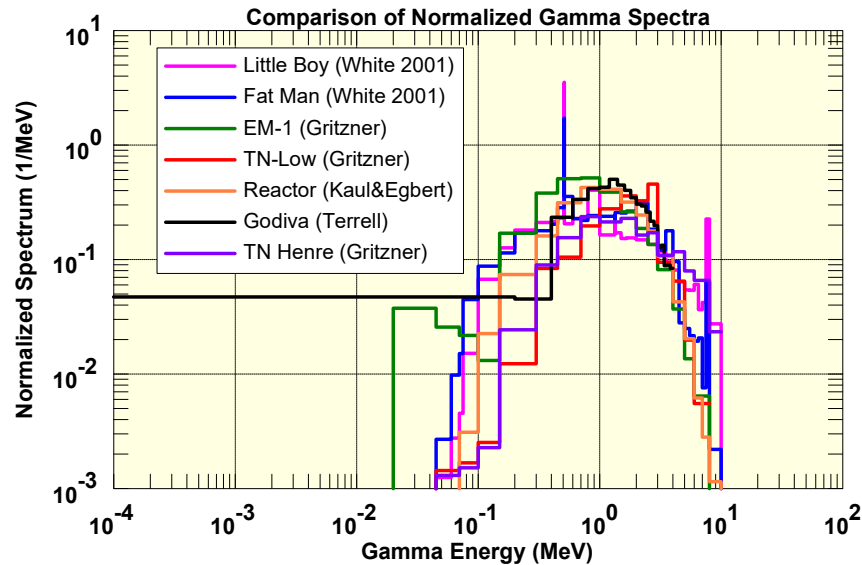

Figure 3. Unclassified gamma spectra from Kramer [13].

4   PARAMETERS AFFECTING HEMP WAVEFORMS

Parameters to consider when determining the strength of HEMP E1 may include the gamma spectrum, high-energy x-ray spectrum, time history of gamma-ray and high-energy x-ray power output, yield, altitude or height of burst (HOB), and the magnetic latitude of the detonation. Below we will examine the sensitivity of the HEMP fields to gamma spectrum, yield, HOB, and the magnetic latitude of the detonation. All calculations assume gamma rays represent 0.2% of the total yield. In all instances, the weapon detonates over a fixed ground location. In the studies looking at the sensitivities to yield and HOB, the gamma spectrum for Fat Man and the (scaled) Glasstone gamma-dot time history is used.

4.1 Gamma Spectrum

To explore the sensitivity of HEMP E1 to gamma spectra, we use for all cases 0.2 kt of gamma rays, which corresponds to a 100 kt device with 0.2% gamma efficiency. In all cases, the weapon detonates above a location near the geographic center of the Continental United States, at 65 km altitude. Figure 4 depicts the incident HEMP E1 field for the seven spectra shown in [13], in both logarithmic and linear vertical scales. We see that the HEMP E1 waveforms in Figure 4 all show very similar shapes. All the peaks fall within 32 kV/m ± 4 kV/m. In general, HEMP E1 is fairly insensitive to the gamma spectra.
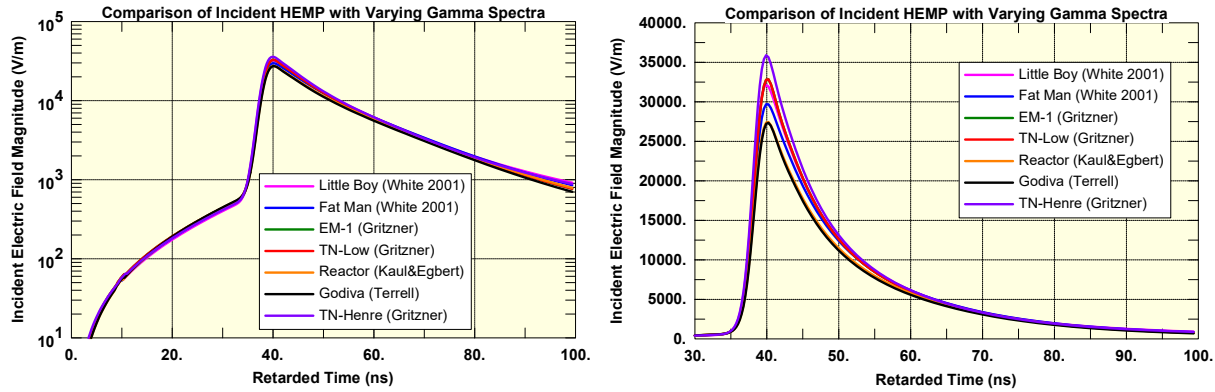

Figure 4. Logarithmic (left) and linear (right) plots of predicted incident HEMP E1 magnitudes as a function of (retarded) time, for a nuclear detonation at 65 km above a location near the geographic center of the Continental United States, for all seven spectra in [13].

4.2 Yield and Height of Burst

Dependence of HEMP E1 on yield and altitude are intertwined. This is because a higher yield weapon can drive HEMP E1 fields to saturation from a much higher detonation altitude than a significantly lower yield weapon. Therefore, one expects the maximum HEMP E1 on the ground to occur for lower heights of burst for lower yields.

4.2.1 Incident HEMP E1 Footprints for 100 kt for Different Heights of Burst

Figure 5 shows contours for the incident HEMP E1 on the ground from a 100 kt detonation over the same central US location at 80 km, 65 km, and 50 km, with peak electric fields at 34 kV/m, 36 kV/m and 32 kV/m, respectively. The footprint gets smaller with decreasing height of burst. This is solely due to the decrease in field of view with decreasing altitude. In these three cases, the maximum field on the ground occurs for the intermediate height of burst of 65 km. Because this is the northern hemisphere, the peak is to the south, and the minimum is to the north. The reverse would true in the southern hemisphere.
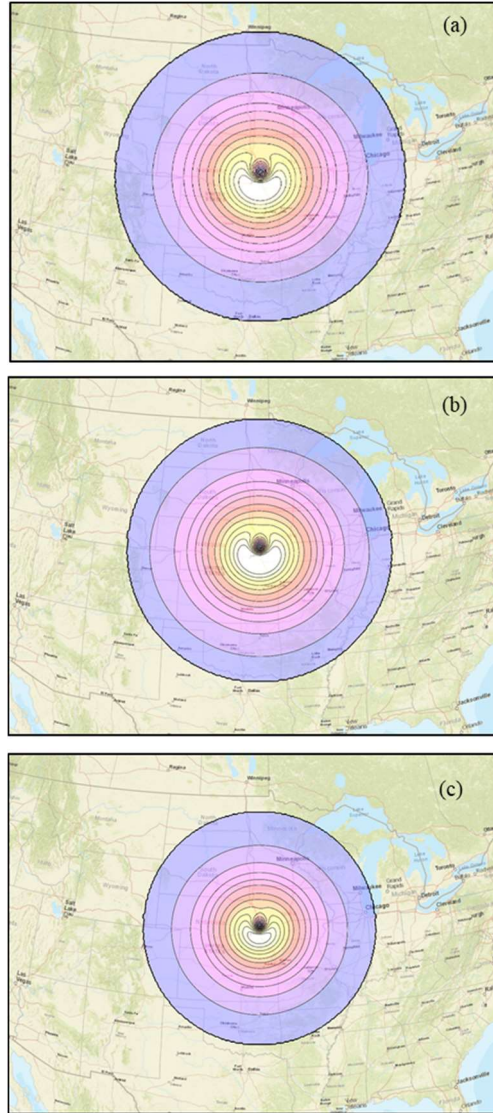
Figure 5. The incident electric field E, in units of kilovolts per meter (kV/m), for a 100 kt nuclear detonation over a location near the geographic center of Continental United States at altitudes of 80 km (a), 65 km (b), and 50 km (c). The rings are in intervals of 2 kV/m, with the outermost ring at 4 kV/m in all three instances. The peak incident field values for all time are 34 kV/m (a), 36 kV/m (b), and 32 kV/m (c), respectively.

4.2.2   Incident HEMP E1 in North-South Plane for 65 km HOB While Varying Yield

To understand the dependence of HEMP E1 values on the ground versus yield, it is better to look at the HEMP E1 fields throughout the atmosphere. This is done by looking at the contours in a north-south plane aligned with the (local) magnetic field[3]. Figure 6 shows a series of E1 field plots for weapons yields of 10 kt, 30 kt, 100 kt, 300 kt, and 1000 kt. For the lowest yields, the gamma-ray intensity is too low to build fields up to the saturation level. As yields increase above 100 kt

---

[3] Based on the 2015 World Magnetic Model (WMM), the geomagnetic field in the vicinity of 41°N, 68°W has a magnitude of approximately 53 micro-tesla (μT), with a declination of 2° to the east of the true magnetic north and a dip angle ("inclination") of 68°.

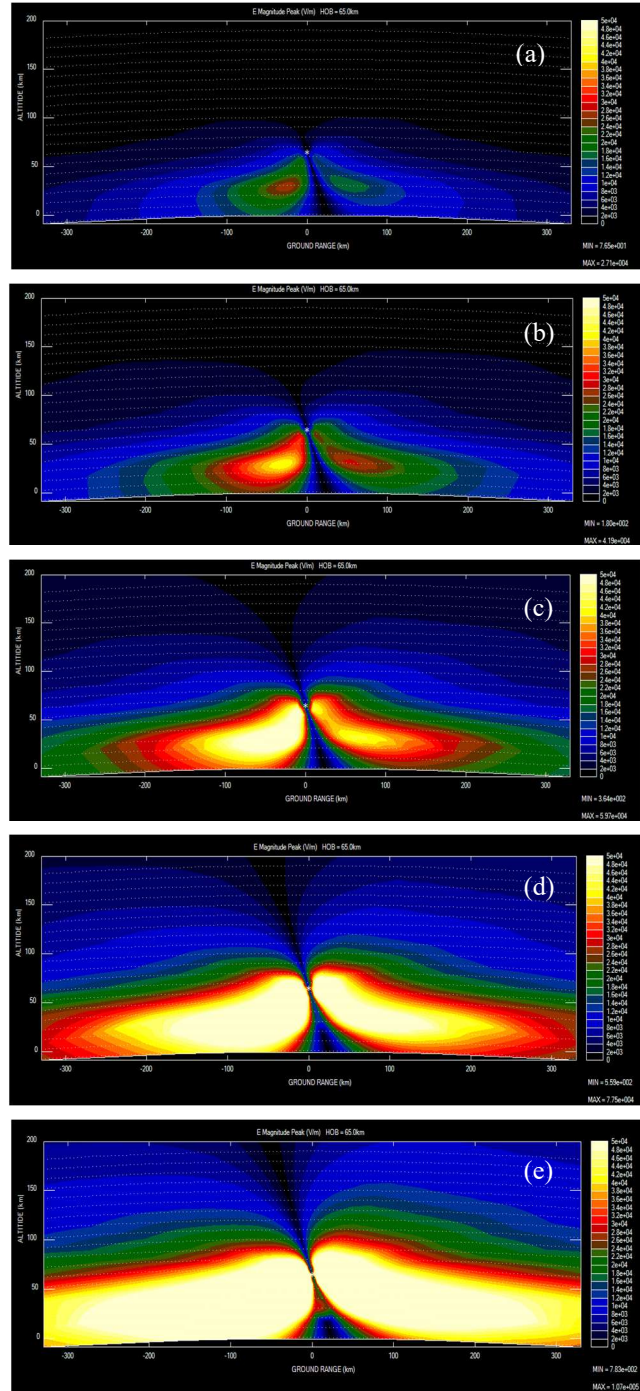for this burst altitude, the fields become saturated, eventually peaking at around 50 kV/m on the ground.

Figure 6. The north-south slice of the HEMP field, plotted against the distance from ground zero, for a nuclear detonation at 65 km above Continental US, for weapons yields of 10 kt (a), 30 kt (b), 100 kt (c), 300 kt (d), and 1000 kt (e).

4.2.3 Incident HEMP E1 in North-South Plane While Varying Height of Burst and Yield

HEMP E1 dependence on height of burst is intertwined with yield, so it is important to examine both. Figure 7 shows the contours for various heights of burst ranging from 20 to 90 km. For each altitude, three yields, 10 kt, 100 kt, and 1000 kt, are studied. The strongest HEMP E1 comes in directions that cross the geomagnetic field orthogonally; however, depending on the altitude, this may not be in the downward direction. For detonations at 20 km, the strongest HEMP E1 is upward since the atmosphere underneath is too dense to form a strong HEMP E1. For 30 km, the strongest HEMP E1 is sideways through the atmosphere; HEMP E1 fields in the 10 km to 50 km layer are intense, but fields on the ground are not as strong as higher altitudes. As the height of burst increases from 50 km to 90 km, the HEMP E1 becomes increasingly directed toward the ground; for lower yields at these altitudes, the HEMP E1 ultimately becomes weaker due to the intensity of the gamma rays being too weak when they reach the conversion layer between 20 km and 40 km. For the 10 kt case, the strongest fields on the ground occur for heights of burst around 50 km, while for 100 kt, the strongest fields on the ground occur for heights of burst near 60 km. For the 1000 kt, the maximum fields on the ground occur for detonation height of approximately 90 km.
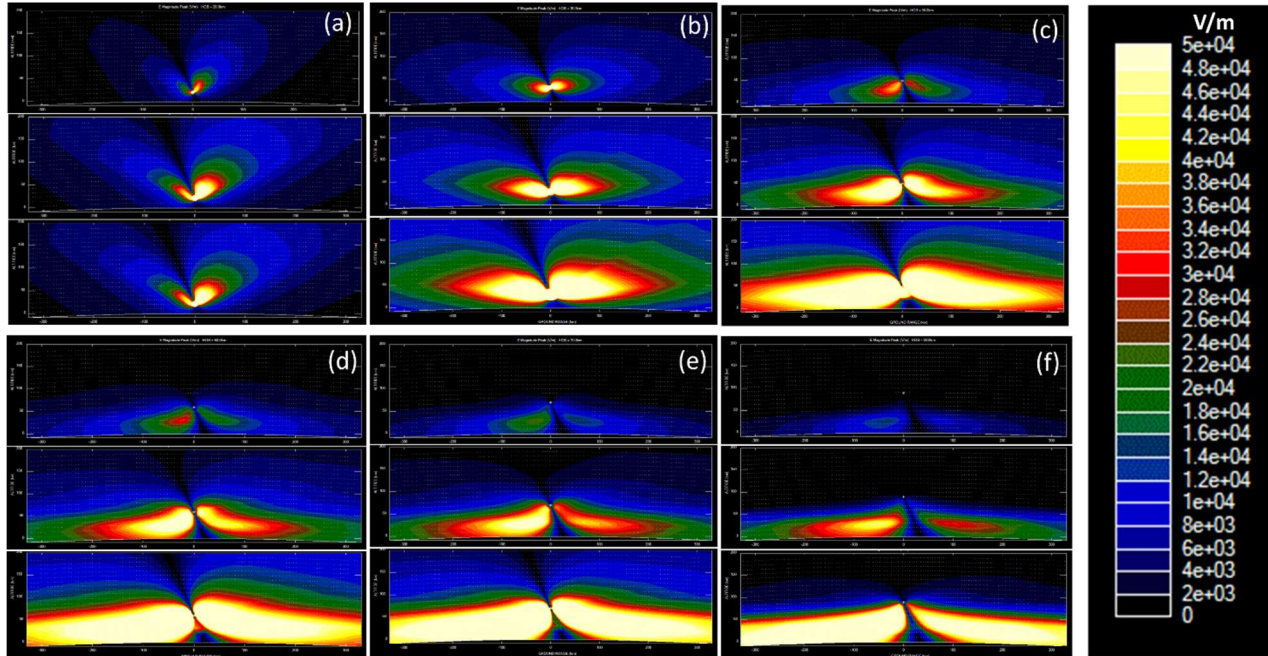

Figure 7. The intertwined effects of yield and HOB: North-south contours for detonations at 20 km (a), 30 km (b), 50 km (c), 60 km (d), 70 km (e), and 90 km (f), for yields of 10 kt (top), 100 kt (middle), and 1000 kt (bottom).

4.2.4 Latitude

The peak HEMP E1 field on the surface does not vary significantly over the 48 contiguous states, but it does trend downward from the Canadian border in the north to the Mexican border in the south. The shape of the contour footprint on the ground, the "smile" contours, also shifts as the angle of the earth's magnetic field goes from more vertical in the north to more horizontal in the south. Figure 8 and Figure 9 show the ground contours and contours on the north-south cut plane, respectively, for a nominal 100 kt detonation at 65 km burst altitude above a location near the US-

Canadian border, a location over central US, ; and a location near the US-Mexican border. The peak E-field values are 36 kV/m, 36kV/m, and 34 kV/m, respectively.
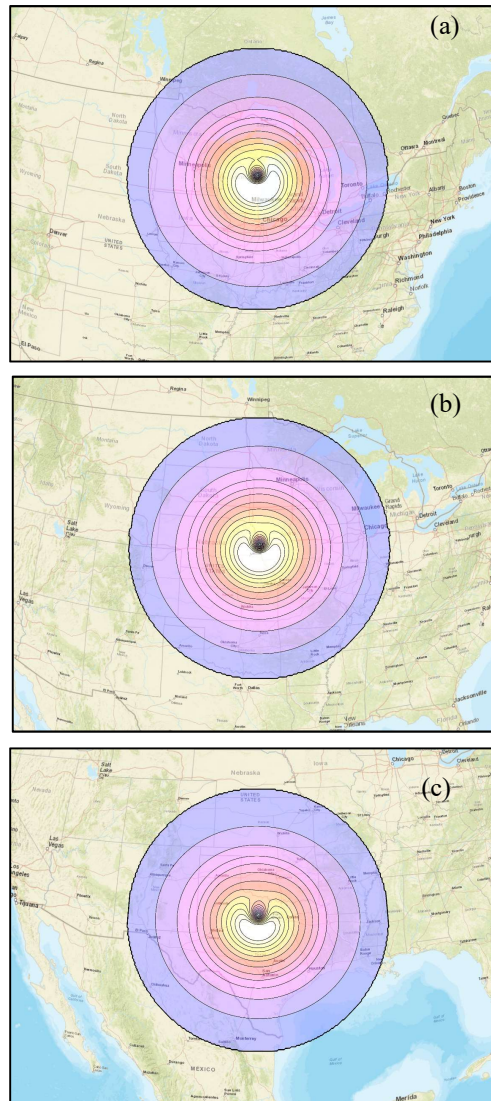

Figure 8. The ground contours of the E1 peak field for a 100 kt detonation at 65 km above points at northern (a), central (b), and southern (c) Continental US.
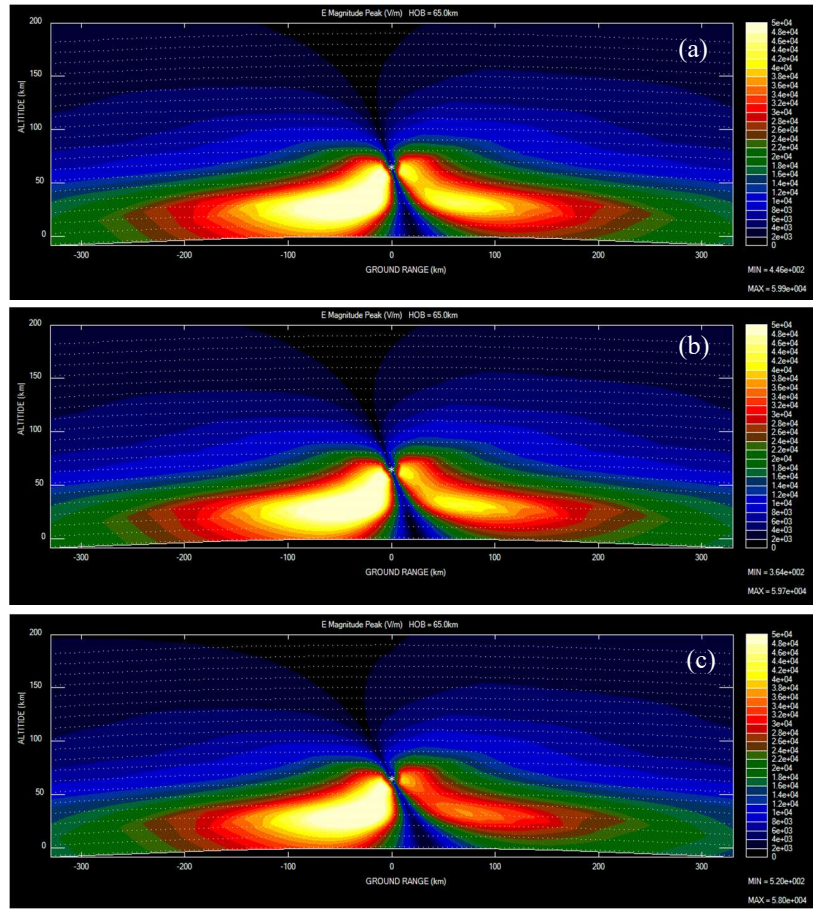
Figure 9. The north-south plane contours of the E1 peak field for a 100 kt detonation at 65 km above points at northern (a), central (b), and southern Continental US.

5 MAXIMUM INCIDENT HEMP E1 WAVEFORMS

Figure 10 shows the waveforms (magnitude of the electric field as a function of time) in linear and logarithmic vertical scales for the maximum incident HEMP E1 for the various yields for detonations above US. For each yield, there is an optimal height of burst that produces the maximum HEMP E1, as well as the angle from the nadir (the point directly below burst point), pointing to the south, that produces the maximum field. From these plots we see that the waveform becomes faster rising and narrower along with a larger peak as the yield increases. These metrics are captured in Table 1, which lists the peak incident field, the 10%-90% rise time, the full width at half maximum (FWHM), and the height of the burst (HOB) for the yield.
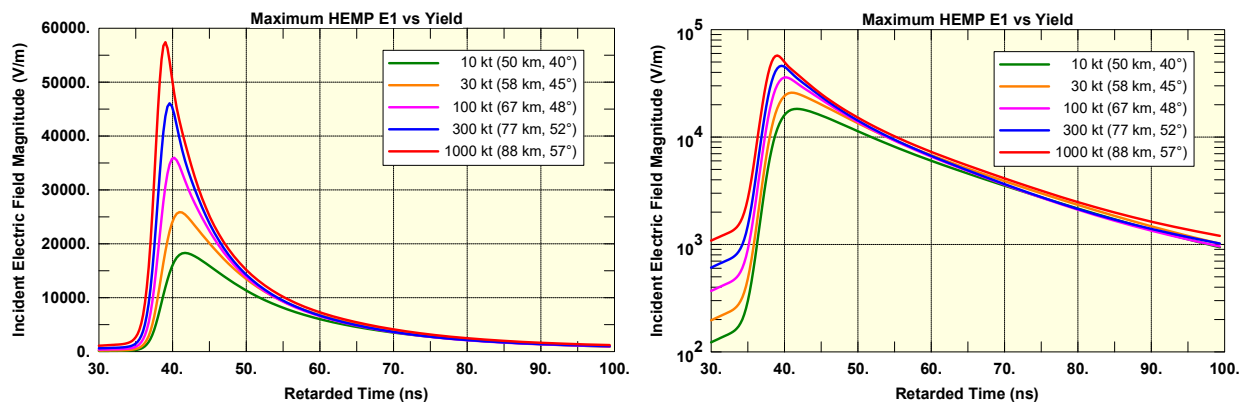

Figure 10. Waveforms for the maximum incident HEMP E1 for yields from 10 kt to 1000 kt, on the linear (left) and logarithmic (right) scales. The numbers in the parentheses give the height of burst for the maximum field, and the nadir angle from the detonation in the southward direction that generates the maximum incident field.

Table 1. List of HEMP E1 maximum waveforms as a function of yield.

Yield (kt)	E_{peak} (kV/m)	t_{rise} (ns)	FWHM (ns)	HOB (km)
10	18	3	15	50
30	26	3	12	58
100	36	3	9	67
300	46	3	8	77
1000	57	2	7	88

6 REFERENCES

[1] C. L. Longmire, "On the Electromagnetic Pulse Produced by Nuclear Explosions," *IEEE Transactions on Antennas and Propagation,* Vols. AP-26, no. 1, pp. 3-13, January 1978.

[2] "United States Nuclear Tests: July 1945 through September 1992, DOE/NV-209-REV 16," U. S. Department of Energy, National Nuclear Security Administration Nevada Field Office, 2015.

[3] W. J. Karzas and R. Latter, "Electromagnetic Radiation from a Nuclear Explosion in Space," *Physical Review,* vol. 126, p. 1919, 1962.

[4] J. D. Jackson, Classical Electrodynamics, 3rd ed., John Wiley & Sons, 1998.

[5] C. L. Longmire and H. J. Longley, "Improvements in the Treatment of Compton Current and Air Conductivity in EMP Problems," Defense Threat Reduction Agnecy, Washington, DC, 1973.

[6] C. E. Baum, "Air Conductivity: Some New Developments," EMP Theoretical Note 2, 1965.

[7] C. L. Longmire and J. Koppel, "Formative Lag of Secondary Ionization," Defense Threat Reduction Agency, Washington, DC, 1974.

[8] A. V. Phelps, "Laboratory studies of electron attachment and detachment process of aeronomic interest," *Canadian Journal of Chemistry,* vol. 47, pp. 1783-1793, 19769.

[9] V. van Lint, "Electron Mobility and Attachment Rate in Dry and Moist Air," Defense Threat Reduction Agency, Washington, DC, 1982.

[10] H. J. Longley and Longmire, C. L., "Development of CHAP -- a High-Atitude EMP Code," Defense Nuclear Agency, Washington, DC, January 1978.

[11] S. Glasstone and P. J. Dolan, The Effects of Nuclear Weapons, 3rd ed., U.S. Department of Defense and U.S. Department of Energy, 1977.

[12] S. W. White and R. L. Holmes, "Standardized Unclassified Little Boy and Fat Man Outputs," Defense Threat Reduction Agency, Washington, DC, September 2013.

[13] K. Kramer, T. Dant, A. Li and K. Millage, "Publicly Released Prompt Radiation Spectra Suitable for Nuclear Detonation Simulations," Defense Threat Reduction Agency, April 2017.